A Low-Cost High-Gain Dual-Beam Antenna With Large Beam Tilt Angle for Through-Wall FTTR Applications

Dian Li, Xulin Xu, Long Zhang, *Member, IEEE*, Hao Xiong, Dongwei Wu, Francis Keshmiri, Xiang Wang, Wenchao Liu, Yejun He, *Senior Member, IEEE*, and Steven Gao, *Fellow, IEEE*

***Abstract*—In this letter, a high-gain dual-beam antenna with large beam tilt angle is proposed as a cost-effective solution for through-wall fiber-to-the-room (FTTR) applications. The dual-beam radiation is realized by the antiphase currents distribution on the antenna, and two pairs of parasitic elements are loaded to significantly elevate the beam tilt angle and improve the bandwidth. The measured bandwidth of the proposed antenna is 1100 MHz (4.88 GHz to 5.98 GHz), well covering the FTTR operation bands. Besides, the maximum tilt angle for the symmetrical dual beams reaches 53°, and the peak gain is 10.05 dBi at 5.3 GHz. Moreover, received signal strength indicator and throughput experiments are conducted to verify the efficacy of the proposed antenna in terms of through-wall functionality. The experimental results demonstrate that the proposed antenna exhibits superior through-wall and multiroom coverage capability in comparison to the conventional monopole antenna.**

***Index Terms*—Dual-beam antenna, fiber-to-the-room (FTTR) antenna, high gain, large beam tilt angle, multiroom coverage, through-wall.**

I. Introduction

In scenarios where rooms are arranged closely, such as dormitories and hotels, the propagation of electromagnetic waves will be greatly attenuated across the walls of adjacent rooms, leading to a wireless access point (AP) equipped per room for better communication service. Therefore, the deployment of a single AP to cover multiple rooms has received considerable interests due to the significant reduction of network construction cost [1]. Dual-beam antennas are well-suited for wireless systems that require the coverage of multiple areas simultaneously [2]. As illustrated in Fig. 1, a ceiling-mounted dual-beam antenna with large beam tilt angle and high antenna gain can effectively extend the signal coverage area from one room to three rooms. However, achieving signal coverage over such an extensive area is quite challenging for antenna design: 1) the dual beams of the antenna need to have a large beam tilt angle (approximately 50° to 55°) to cover rooms on both sides of a wall; 2) it is imperative that the antenna possesses high gain over a wide beamwidth for better through-wall coverage [3], [4], specifically the beamwidth with gain $>$ 4 dBi should be greater than 40°; 3) the bandwidth of the antenna needs to cover the fiber-to-the-room (FTTR) 5 GHz band while the antenna structure needs to be as simple as possible for cost and compatibility purpose.

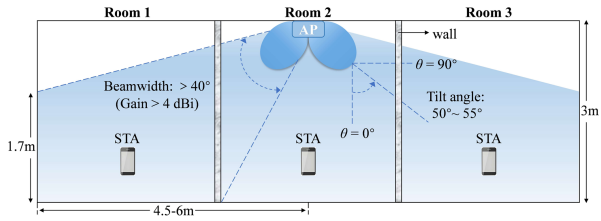

Fig. 1. Schematic of multiroom coverage utilizing high-gain dual-beam antennas (adjacent rooms are separated by a wall).

Usually, dual-beam radiation can be achieved by elaborately designed back-to-back endfire antennas [5], [6], [7], [8], phased array antennas [9], [10], [11], [12], [13], leaky-wave antennas [14], [15], [16], [17], [18], and microstrip antennas [19], [20], [21], [22], [23], [24]. For back-to-back endfire antennas, the dual beams pointing to opposite directions are incapable of covering multiple rooms when the antenna is installed on the rooftop. Phased array antennas are not suitable for ceiling-mounted applications due to their complex and costly system architecture, while leaky-wave antennas are incompatible for FTTR scenarios where the spectrum resources are quite limited for each channel. Although microstrip antennas have been widely used to generate dual-beam radiation, they suffer from drawbacks of narrow bandwidth, small beam tilt angle and low antenna gain. A dual-beam antenna with large beam tilt angle was reported in [25]. However, the antenna comprises six independent steel plates and a feeding network on the ground plane, which renders it disadvantageous in terms of design simplicity, fabrication cost, and assembly accuracy, and not applicable to practical applications.

Received 29 July 2025; revised 27 August 2025; accepted 10 September 2025. Date of publication 17 September 2025; date of current version 18 December 2025. This work was supported in part by the National Key Research and Development Program of China under Grant 2023YFE0107900, in part by the the Shenzhen Science and Technology Program under Grant JCYJ20230808105510020, in part by the Key Program of Shenzhen Natural Science Foundation under Grant JCJY20241202124219023, and in part by Huawei under Grant TC20230808040. *(Corresponding author: Long Zhang.)*

Dian Li, Xulin Xu, Long Zhang, and Yejun He are with the College of Electronics and Information Engineering, Shenzhen University, Shenzhen 518060, China (e-mail: zhang@szu.edu.cn).

Hao Xiong, Dongwei Wu, Francis Keshmiri, and Xiang Wang are with the Huawei Technologies Company Ltd., Shenzhen 518100, China (e-mail: xionghao30@huawei.com; wudongwei2@huawei.com; francis.keshmiri@huawei.com; eric.wangxiang@huawei.com).

Wenchao Liu is with the Home Network Department, E-surfing Digital Life Technology, China Telecom, Shanghai 200061, China (e-mail: liuwc_dys.sh@chinatelecom.cn).

Steven Gao is with the Department of Electronic Engineering, The Chinese University of Hong Kong, Hong Kong (e-mail: scgao@ee.cuhk.edu.hk).

Digital Object Identifier 10.1109/LAWP.2025.3610997

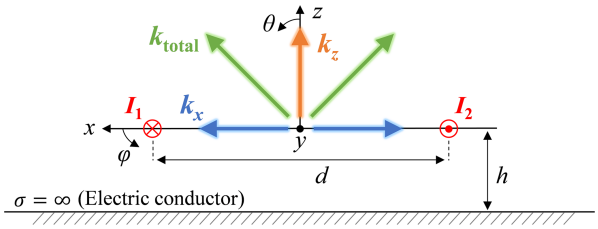

Fig. 2. Illustration of two antiphase electric currents array.

Based on the above discussion, this letter proposes a high-gain, broadband, dual-beam antenna with large beam tilt angle for through-wall FTTR applications. The dual-beam radiation is realized by exciting two antiphase currents, then two pairs of parasitic elements are introduced to further elevate the beam tilt angle and extend the bandwidth. The measured results show that the antenna can achieve symmetrical dual beams with a beam tilt angle greater than 50° and the realized gain exceeding 9 dBi within the 5 GHz to 5.9 GHz band. Comprehensive system experiments, including the received signal strength indicator (RSSI) and throughput measurements, verify the antenna as an excellent solution for through-wall FTTR applications.

II. Antenna Design and Principle

Let us consider a two-element array made up of two antiphase electric currents placed along the y-axis direction, as shown in Fig. 2. The far-field pattern of a single electric current is defined as [26]

$$E_0(\varphi) = j\eta \frac{kI_0 l \cos\varphi}{4\pi r} e^{-jkr} \tag{1}$$

where η is the wave impedance, $k = 2\pi/\lambda$ is the free-space wavenumber, I_0 is the current amplitude, and l is the current length. Then, the array factor for the two elements array with the same magnitude and phase difference β is

$$AF = \cos\left[\frac{1}{2}(kd\sin\theta\cos\varphi + \beta)\right] \tag{2}$$

where $\beta = \pi$. For the xz-plane and yz-plane, φ equals 0 and $\pi/2$, respectively. Thus, the total far-field patterns for the antiphase currents in the two main planes are

$$E(\theta,\varphi)_{xz} = -E_0 \sin\left(\frac{kd}{2}\sin\theta\right), E(\theta,\varphi)_{yz} = 0. \tag{3}$$

If $d \approx \lambda/2$, then the maximum radiation is obtained in the x-axis direction (denoted by k_x), while the radiation in the y-axis direction is canceled out. Once an electric conductor is placed underneath, the reflected waves induced by the conductor will be oriented along the z-axis direction (denoted by k_z) according to the image theory. Thus, the total wave vector k_{total} is superposed by k_x and k_z, generating a tilted dual-beam radiation. By adjusting the radiation intensity along vector k_x and k_z, the beam tilt angle can be altered.

Based on the aforementioned principles and inspired by the horizontally polarized antenna presented in [27], a dual-beam antenna with improved bandwidth and gain is proposed. The configuration of the proposed dual-beam antenna is shown in Fig. 3, which consists of a meander line, a notch radiator, two symmetrical rectangular strips, two symmetrical trapezoidal directors, and a ground plane. All elements are printed on an FR4 substrate ($\varepsilon_r = 4.4$) with a thickness of 0.762 mm. The ground

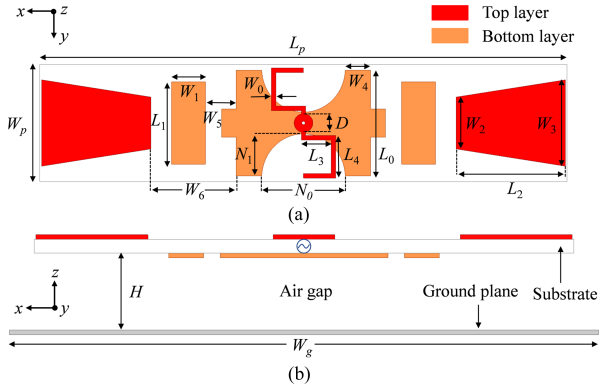

Fig. 3. Configuration of the dual-beam antenna. (a) Top view. (b) Side view. Design parameters (unit: mm): $L_p = 96$, $W_p = 21$, $W_0 = 0.8$, $W_1 = 6.2$, $W_2 = 9.5$, $W_3 = 15.8$, $W_4 = 4.6$, $W_5 = 5.6$, $W_6 = 15.5$, $W_g = 126$, $L_0 = 19.3$, $L_1 = 15$, $L_2 = 20$, $L_3 = 5.5$, $L_4 = 7$, $N_0 = 15.2$, $N_1 = 7.6$, $D = 3.4$, and $H = 14.5$.

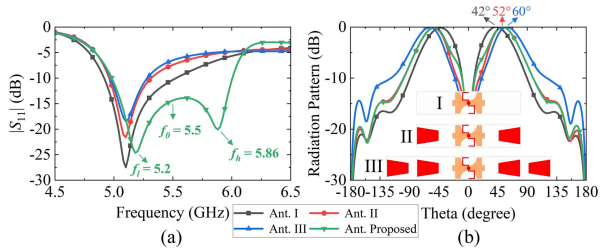

Fig. 4. (a) Simulated $|S_{11}|$ of Ant. I–III and proposed. (b) Simulated radiation patterns in xz-plane for Ant. I–III and proposed at 5.1 GHz.

plane is printed on another FR4 substrate, while two dielectric substrates are separated by an air gap with a height H, and a coaxial cable is used to feed the antenna directly.

The meander line provides differential excitation to the notch radiator, creating antiphase electric currents on the radiator. Therefore, radiation nulls along the y-axis occur, while high-gain dual-beam radiation is generated in the x-axis direction. To illustrate the role of the trapezoidal directors, the antenna with only the notch radiator and the meander line is denoted as Ant. I. Ant. II refers to Ant. I plus a pair of trapezoidal directors, while Ant. III refers to Ant. I plus two pairs of trapezoidal directors. The trapezoidal shape is chosen over the rectangular one because its gradual taper can expand the operating bandwidth of the directors. As shown in Fig. 4, Ant. I–III resonate at 5.1 GHz, and the tilt angle of the symmetrical dual beams in the xz-plane is 42° for Ant. I, 52° for Ant. II, and 60° for Ant. III. This indicates the trapezoidal directors can enhance the radiation intensity along vector k_x, thus elevating the beam tilt angle effectively. Similarly, the magnitude of k_z can be adjusted by changing the antenna height H to fine-tune the beam tilt angle. Meanwhile, loading the trapezoidal directors enhances the endfire radiation, thereby improving the gain by about 1 dB. Since Ant. II has a suitable beam tilt angle that satisfies the system requirements, a single pair of trapezoidal directors is chosen.

As the bandwidth of Ant. II is too narrow to cover the FTTR 5 GHz band (5.15 GHz to 5.85 GHz), a pair of rectangular strips is added on either side of the notch radiator, which can introduce an additional resonance at 5.86 GHz (f_h) while the resonance generated by the notch radiator only shifts slightly from 5.1 GHz to 5.2 GHz (f_l). As shown in Fig. 5(a), the surface currents at 5.2 GHz are predominantly concentrated on the notch radiator, indicating that the radiation mainly comes from the

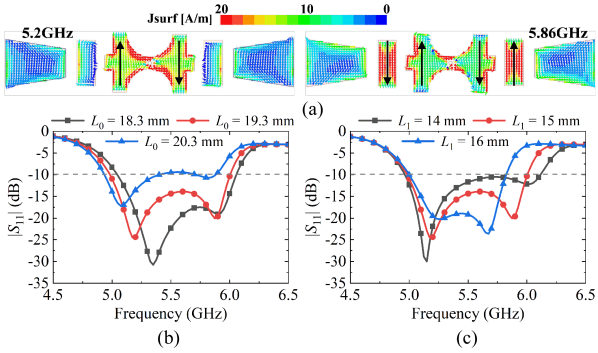

Fig. 5. (a) Current distributions of the proposed antenna at 5.2 GHz and 5.86 GHz. (b) Simulated $|S_{11}|$ for different L_0. (c) Simulated $|S_{11}|$ for different L_1.

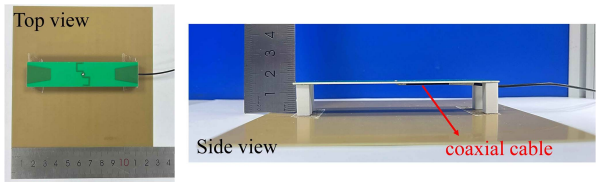

Fig. 6. Photographs of the fabricated dual-beam antenna.

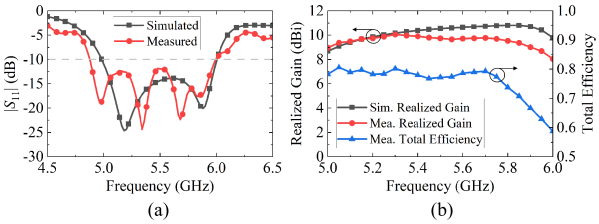

Fig. 7. Simulated and measured results of the proposed dual-beam antenna. (a) $|S_{11}|$. (b) Realized gain and total efficiency.

notch radiator. Whereas at 5.86 GHz, the surface currents on the rectangular strips are significantly enhanced, indicating both the rectangular strips and the notch radiator contribute to the radiation, thus significantly expanding the bandwidth from 340 MHz (4.96 GHz to 5.3 GHz) to 1000 MHz (5 GHz to 6 GHz). It is necessary to note that the rectangular strips have a limited effect on the radiation pattern and the antenna gain.

The proposed antenna is, in principle, similar to the Yagi antenna. Thus, the initial dimensions of the antenna can be set as follows: $L_0 \approx \lambda_l/2$, $L_1 \approx \lambda_h/2$, $N_0 + W_4 \times 2 \approx \lambda_0/2$, $W_6 \approx \lambda_0/4, W_2 < 0.4\lambda_h, W_3 > 0.4\lambda_l$, and $L_2 \approx 0.4\lambda_0$ (λ_l and λ_h are the guided wavelength at f_l and f_h, respectively, while λ_0 is the free-spcae wavelength at f_0). Fig. 5 shows a further study on the length of the notch radiator (L_0) and the rectangular strips (L_1). As L_0 increases, the resonance of the notch radiator is shifted to lower frequency, while the resonance of the rectangular strips is almost kept unchanged. Similarly, the resonance of the rectangular strips is moved to lower frequency when increasing L_1, while the resonance of the notch radiator remains essentially stable.

III. Antenna Measurement Results and Discussion

An antenna prototype is fabricated and measured, as shown in Fig. 6. Fig. 7(a) shows the simulated and measured reflection coefficients, demonstrating bandwidths of 1000 MHz (5 GHz to 6 GHz) and 1100 MHz (4.88 GHz to 5.98 GHz), respectively.

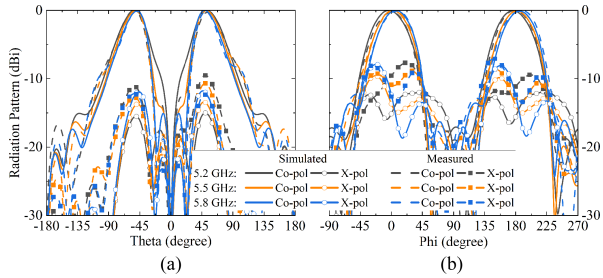

Fig. 8. Simulated and measured normalized radiation patterns of the proposed antenna in (a) xz-plane and (b) theta = 52° plane at 5.2 GHz, 5.5 GHz, and 5.8 GHz.

TABLE I
Comparison With Previously Reported Dual-Beam Antennas

Ref.	BW (%)	BTA (°)	Gain (dBi)	Beamwidth (°) Ele./Azi.	Dimensions (λ_0^3)
[20]	13.2	32.5	8.87	∼45/N.A.	1.83×1.28×0.1
[21]	12.7	31	7.7	∼45/N.A.	1.14×0.7×0.17
[22]	23.5	30	6.8	∼38/N.A.	1.13×0.42×0.09
[23]	7.3	33	9.6	∼40/N.A.	1.63×1.63×0.05
[24]	6	46	7.3	∼35/N.A.	2.27×2.27×0.05
[25]*	16	54	8.9	48/64	1.76×1.11×0.24
Prop. SG*	18.2	53	9.8	57/72	1.76×1.11×0.24
Prop.	**20.3**	**53**	**10.05**	**49/72**	**2.3×2.3×0.27**

*: simulation results; BW: bandwidth; BTA: beam tilt angle; SG: small ground; ∼: approximately equal to; N.A.: not available; Ele.: elevation plane; Azi.: azimuth plane; Beamwidth refers to the beamwidth with gain > 4 dBi.

The difference between the simulated and measured reflection coefficients is caused by the fabrication and measurement errors, especially the possible reflections of the coaxial cable (25 cm long) and IPEX-to-SMA transition. As depicted in Fig. 7(b), the realized gain exceeds 9 dBi within the 5 GHz to 5.9 GHz band, with a maximum gain of 10.05 dBi at 5.3 GHz. The total efficiency surpasses 70% within the 5 GHz to 5.85 GHz band, with a maximum efficiency of 80.62% at 5.05 GHz.

The simulated and measured normalized radiation patterns at 5.2 GHz, 5.5 GHz, and 5.8 GHz in the xz-plane (elevation plane) and theta = 52° plane (azimuth plane) are shown in Fig. 8. The measured results demonstrate that the tilt angles of the symmetrical dual beams are all greater than 50° at various frequencies, with a maximum tilt angle of 53° at 5.2 GHz.

In addition to the beam tilt angle, beamwidth is also a critical metric for practical application. The measured beamwidths for gain > 4 dBi in the xz-plane at 5.2 GHz, 5.5 GHz, and 5.8 GHz are 49°, 45°, and 43°, respectively, satisfying the requirements delineated in Fig. 1. For the theta = 52° plane, the measured beamwidths are all greater than 72°. A comparison of the proposed and previously reported dual-beam antennas is tabulated in Table I. As revealed by Table I, the proposed antenna is superior to previous designs in terms of beam tilt angle, gain, and beamwidth. Although the proposed antenna has a large ground plane due to the system requirement, the antenna performance remains essentially unchanged except for a slight decrease in antenna gain under the same size, as in [25].

IV. RSSI and Throughput Experimental Results

A conventional monopole antenna with conical-beam radiation is fabricated and selected as the reference antenna for system experimental results comparison. The impedance bandwidth and the radiation patterns of the monopole antenna are shown in

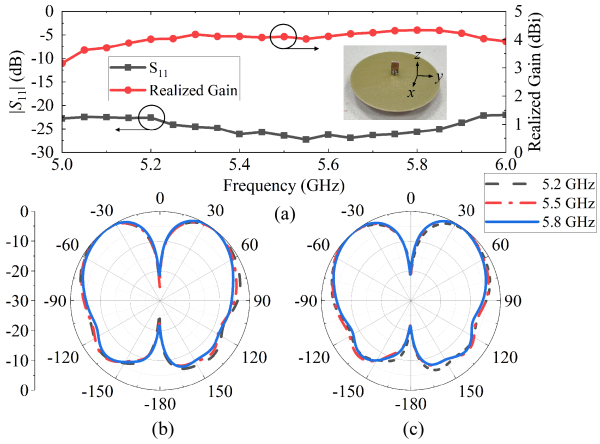

Fig. 9. Measured results of the monopole antenna. (a) $|S_{11}|$ and realized gain. (b) and (c) Normalized radiation patterns in *xz*-plane and *yz*-plane.

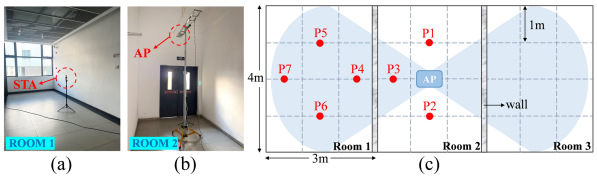

Fig. 10. Experimental scenarios for RSSI and throughput. (a) Room 1. (b) Room 2. (c) Top view of the testing scenario.

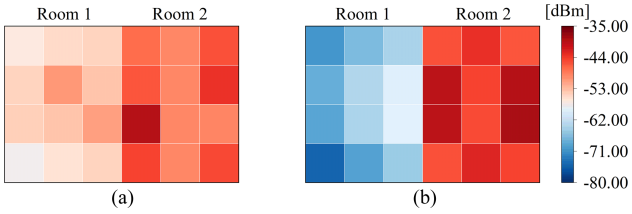

Fig. 11. RSSI distribution in Room 1 and Room 2 for (a) the proposed dual-beam antenna and (b) the monopole antenna.

Fig. 9. Within the operation band of 5 GHz to 6 GHz, the measured $|S_{11}|$ is less than -20 dB. Conical beams with a maximum gain around theta $= 40°$ in both main planes are observed. The measured realized gain of the monopole antenna is greater than 4 dBi from 5.2 GHz to 5.95 GHz.

The scenario, as shown in Fig. 10, is chosen for RSSI and throughput experiments. To better characterize the experimental results, each room is divided into 12 square cells. Due to the symmetry of the experimental site, only the left half is selected for results demonstration (Rooms 1 and 2). The AP, located at the center of Room 2, is placed 3 m above the ground and 1.5 m from the 25 cm-thick reinforced concrete wall. A mobile phone placed 1.2 m above the ground functions as a station to connect to the AP. The mean RSSI value over a 1 min period is measured at the center of each cell in Rooms 1 and 2, while throughput is measured at seven sampling points, as indicated by red dots in Fig. 10(c).

The distribution of RSSI in Rooms 1 and 2 is illustrated in Fig. 11. The omnidirectional radiation of the monopole antenna with a small beam tilt angle ensures effective signal coverage in a single room, therefore, the RSSI levels of the dual-beam antenna within Room 2 are slightly lower than that of the monopole antenna due to the large beam tilt angle. Whereas in Room 1, the RSSI levels of the monopole antenna drop dramatically,

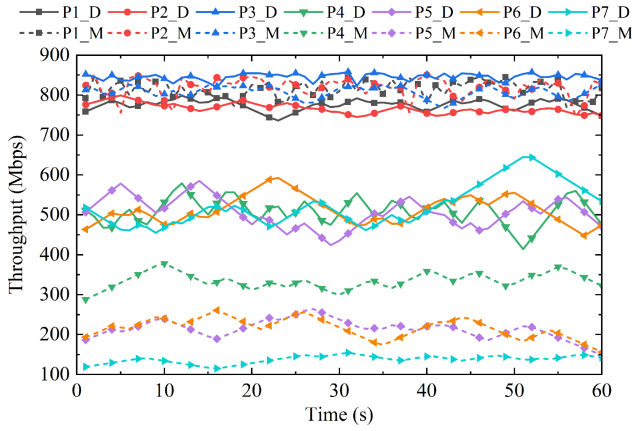

Fig. 12. Throughput results tested in 1 min (D for the dual-beam antenna and M for the monopole antenna).

particularly at the room corners, while the dual-beam antenna can still maintain the RSSI levels above -58 dBm throughout the room for better communication service. The RSSI of the proposed dual-beam antenna exhibits slight asymmetry within Room 2 due to its nonstatic nature, which can be modeled as a Gaussian random variable [28], as well as the beam pointing errors caused by the possible nonideal placement of the antenna.

The modulation and coding scheme index selected for throughput measurement is 11, which corresponds to 1024-QAM modulation, as defined by the wireless network protocol IEEE 802.11ax. In this case, the maximum code rate is 5/6, the number of subcarriers is 2×980, and the maximum bandwidth is 160 MHz (one spatial stream), corresponding to a theoretical maximum throughput of 1201 Mbps. Usually, the actually measured throughput typically falls short of the theoretical limit, due to factors, such as antenna performance, polarization mismatch, and ambient noise. The throughput measured at each sampling point is shown in Fig. 12. Although the throughput of the dual-beam antenna is slightly lower than that of the monopole at P1 and P2, it still exceeds 736 Mbps. In Room 1, the throughput of the dual-beam antenna are all greater than 414 Mbps, whereas the throughput of the monopole antenna gradually declines with distance and is less than 150 Mbps at P7. Overall, the proposed antenna demonstrates strong through-wall performance even under such high-attenuation conditions. For low attenuation environments, such as plywood walls, using the proposed antenna would further enhance coverage, especially in multiroom or corner regions, due to the improved signal penetration capability.

V. Conclusion

This letter proposes a high-gain dual-beam antenna with large beam tilt angle and broad bandwidth for through-wall FTTR applications. By generating two antiphase electric currents within a single notch radiator, the dual-beam radiation is realized. Subsequently, two pairs of parasitic elements are introduced to achieve large beam tilt angle and broaden the bandwidth. The antenna performance is validated by impedance bandwidth and radiation pattern measurements. Furthermore, RSSI and throughput experiments are also conducted, demonstrating that the proposed antenna has excellent through-wall and multiroom coverage capabilities.

REFERENCES

[1] M. Wu, B. Zhang, Y. Zhou, and K. Huang, "A double-fold 7 × 8 butler matrix-fed multibeam antenna with a boresight beam for 5G applications," *IEEE Antennas Wireless Propag. Lett.*, vol. 21, no. 3, pp. 516–520, Mar. 2022.

[2] K. Wu, Y. Yao, X. Cheng, J. Yu, and X. Chen, "Design of millimeter-wave circularly polarized endfire antenna and multibeam antenna array for wireless applications," *IEEE Trans. Antennas Propag.*, vol. 69, no. 12, pp. 8397–8406, Dec. 2021.

[3] A. Dadgarpour, B. Zarghooni, B. S. Virdee, and T. A. Denidni, "Single end-fire antenna for dual-beam and broad beamwidth operation at 60 GHz by artificially modifying the permittivity of the antenna substrate," *IEEE Trans. Antennas Propag.*, vol. 64, no. 9, pp. 4068–4073, Sep. 2016.

[4] S.-Y. Yin and J.-L. Li, "Reconfigurable antenna with uni- and bidirectional radiation patterns based on metasurface and Fresnel zone plate lens," *IEEE Antennas Wireless Propag. Lett.*, vol. 23, no. 8, pp. 2291–2295, Aug. 2024.

[5] T. Jia and X. Li, "A compact stacked bidirectional antenna for dual polarized WLAN applications," *Prog. Electromagn. Res. C*, vol. 44, pp. 95–108, 2013.

[6] J. Hu, Z.-C. Hao, K. Fan, and Z. Guo, "A bidirectional same sense circularly polarized endfire antenna array with polarization reconfigurability," *IEEE Trans. Antennas Propag.*, vol. 67, no. 11, pp. 7150–7155, Nov. 2019.

[7] H. Guo and W. Geyi, "Design of bidirectional antenna array with adjustable endfire gains," *IEEE Antennas Wireless Propag. Lett.*, vol. 18, no. 8, pp. 1656–1660, Aug. 2019.

[8] J. Hao, J. Ren, X. Du, J. H. Mikkelsen, M. Shen, and Y. Z. Yin, "Pattern-reconfigurable Yagi–Uda antenna based on liquid metal," *IEEE Antennas Wireless Propag. Lett.*, vol. 20, no. 4, pp. 587–591, Apr. 2021.

[9] J. H. Kim and W. S. Park, "A hadamard matrix feed network for a dual-beam forming array antenna," *IEEE Trans. Antennas Propag.*, vol. 57, no. 1, pp. 283–286, Jan. 2009.

[10] X. G. Zhang, W. X. Jiang, H. W. Tian, Z. X. Wang, Q. Wang, and T. J. Cui, "Pattern-reconfigurable planar array antenna characterized by digital coding method," *IEEE Trans. Antennas Propag.*, vol. 68, no. 2, pp. 1170–1175, Feb. 2020.

[11] J. Hu, Z.-C. Hao, and Y. Wang, "A wideband array antenna with 1-bit digital-controllable radiation beams," *IEEE Access*, vol. 6, pp. 10858–10866, 2018.

[12] Y. Zhang, Z. Han, S. Tang, S. Shen, C.-Y. Chiu, and R. Murch, "A highly pattern-reconfigurable planar antenna with 360° single- and multi-beam steering," *IEEE Trans. Antennas Propag.*, vol. 70, no. 8, pp. 6490–6504, Aug. 2022.

[13] Y. Fan et al., "Low-RCS multi-beam metasurface-inspired antenna based on Pancharatnam–Berry phase," *IEEE Trans. Antennas Propag.*, vol. 68, no. 3, pp. 1899–1906, Mar. 2020.

[14] Y. Hou, Y. Li, Z. Zhang, and Z. Feng, "Dual-beam periodic leaky-wave antenna with reduced beam squinting," *IEEE Antennas Wireless Propag. Lett.*, vol. 18, no. 12, pp. 2533–2537, Dec. 2019.

[15] C. Zhang, J. Ren, X. Du, and Y. Yin, "Dual-beam leaky-wave antenna based on dual-mode spoof surface plasmon polaritons," *IEEE Antennas Wireless Propag. Lett.*, vol. 20, no. 10, pp. 2008–2012, Oct. 2021.

[16] Q. Zhang, Q. Zhang, H. Liu, and C. H. Chan, "Dual-band and dual-polarized leaky-wave antenna based on slotted SIW," *IEEE Antennas Wireless Propag. Lett.*, vol. 18, no. 3, pp. 507–511, Mar. 2019.

[17] F. Ge, H. Zhao, S. Li, and X. Yin, "Bidirectional scanning antenna based on surface wave mode," *IEEE Antennas Wireless Propag. Lett.*, vol. 21, no. 8, pp. 1592–1596, Aug. 2022.

[18] D. K. Karmokar, K. P. Esselle, and T. S. Bird, "Wideband microstrip leaky-wave antennas with two symmetrical side beams for simultaneous dual-beam scanning," *IEEE Trans. Antennas Propag.*, vol. 64, no. 4, pp. 1262–1269, Apr. 2016.

[19] A. Khidre, K.-F. Lee, A. Z. Elsherbeni, and F. Yang, "Wide band dual-beam U-slot microstrip antenna," *IEEE Trans. Antennas Propag.*, vol. 61, no. 3, pp. 1415–1418, Mar. 2013.

[20] C. Chen, Y. Guo, and H. Wang, "Wideband symmetrical cross-shaped probe dual-beam microstrip patch antenna," *IEEE Antennas Wireless Propag. Lett.*, vol. 14, pp. 622–625, 2015.

[21] S. Liu, S.-S. Qi, W. Wu, and D.-G. Fang, "Single-feed dual-band single/dual-beam U-slot antenna for wireless communication application," *IEEE Trans. Antennas Propag.*, vol. 63, no. 8, pp. 3759–3764, Aug. 2015.

[22] J.-F. Li, Z. N. Chen, D.-L. Wu, G. Zhang, and Y.-J. Wu, "Dual-beam filtering patch antennas for wireless communication application," *IEEE Trans. Antennas Propag.*, vol. 66, no. 7, pp. 3730–3734, Jul. 2018.

[23] K.-D. Hong, X. Zhang, L. Zhu, and T. Yuan, "A high-gain and pattern-reconfigurable patch antenna under operation of TM_{20} and TM_{21} modes," *IEEE Open J. Antennas Propag.*, vol. 2, pp. 646–653, 2021.

[24] S. Cao, Z. Zhang, X. Fu, and J. Wang, "Pattern-reconfigurable bidirectional antenna design using the characteristic mode analysis," *IEEE Antennas Wireless Propag. Lett.*, vol. 20, no. 1, pp. 53–57, Jan. 2021.

[25] C. Chen, X. Xu, L. Zhang, and F. Keshmiri, "Compact horizontally polarized dual-beam antenna with large tilted beam angle for FTTR applications," in *Proc. 19th Eur. Conf. Antennas Propag.*, Mar. 2025, pp. 1–3.

[26] C. A. Balanis, "Arrays: Linear, planar, and circular," in *Antenna Theory Analysis and Design*, 3rd ed. Hoboken, NJ, USA: Wiley, 2005, ch. 6, pp. 283–286.

[27] B. Rohani, K. Takahashi, H. Arai, Y. Kimura, and T. Ihara, "Improving channel capacity in indoor 4 × 4 MIMO base station utilizing small bidirectional antenna," *IEEE Trans. Antennas Propag.*, vol. 66, no. 1, pp. 393–400, Jan. 2018.

[28] N. Patwari, A. O. Hero, M. Perkins, N. S. Correal, and R. J. O'Dea, "Relative location estimation in wireless sensor networks," *IEEE Trans. Signal Process.*, vol. 51, no. 8, pp. 2137–2148, Aug. 2003.